Li et al. Geoenvironmental Disasters (2015) 2:24
DOI 10.1186/s40677-015-0032-7

Geoenvironmental Disasters
a SpringerOpen Journal

RESEARCH Open Access

Investigation for the initiation of a loess landslide based on the unsaturated permeability and strength theory

Ping Li*, Xingting Zhang and Hao Shi

Abstract

Background: The Yanlian landslide, occurring on 21-22 October 2010, destroyed many facilities of a big oil refinery in Shaan'xi Province, China. It led to a suspending of the refinery work for a week and caused near 700 million RMB economic losses.

Results: Site exploration shows that the sliding mass is unsaturated-saturated loess. The groundwater is rich in the landslide and shortage in the surrounding slopes. Further investigation finds that the water drop released from the vapor heating furnaces on the top of the slope is the only source of the groundwater. Laboratory tests were performed to get the unsaturated strength parameters and hydraulic conductivity of the loess layers which were applied to a pre-failure slope model to simulate the water infiltration process and the stress field based on which the factor of safety is figured out to analyze the slope stability. Analysis shows that during the first ten years, the factor of safety has no prominent decrease. In the following 5 years, the slope stability decreases significantly till failure.

Conclusions: A little water infiltration has minor effects on slope stability for some time. As a result it is easy to be ignored. However, when the period of water infiltration is long enough to raise the groundwater level, it will have detrimental influence on the stability. In conclusion, any minor water produced by engineering or other activities for a long period may have harmful effect on slope stability. Therefore it is essential to take account of this kind of water and adopt measures to curb the surface water infiltration and to drain the groundwater.

Keywords: Unsaturated soil; Loess; Landslide; Strength parameters; Soil-water characteristic curve; Hydraulic conductivity function

Background

Loess landslides occurring in China lead to a huge economic losses every year (Liao et al. 2008; Bai et al. 2012; Li et al. 2012). It has been proved that rainfall, irrigation, water canal leakage, submerging of reservoir, melted snow and earthquake are the main factors triggering loess landslides (Lei, 1994; Dai and Lee 2001; Tu et al. 2009; Li et al. 2013; Zhang & Peng 2014). However, there are no water resources and earthquake mentioned above before the Yanlian landslide occurred, which is located at Luochuan county, Shaanxi province, China as shown in Fig. 1, and the slopes nearby are stable even though they are higher and steeper than the failed. The landslide moves down intermittently for two days and the people working on it has enough time to escape. So there is no fatality in the accident. The cause of the landslide is unclear and deeply concerned by the managers and researchers. The aims of the paper are to find the triggering factors by site exploration and to study the failure mechanism by laboratory tests and numerical analysis.

Methods, results and discussions

Characters of the landslides

The landslide occurred on the erosive bank of the Luohe river which is the second tributary of the Yellow river. The first and the third terraces of the river develop on that bank and the second terrace is eroded off. The first terrace, about 5 m above the river bed, is flat and wide on which there is an oil refinery named Yanlian (Fig. 2). Against the rear of the first terrace is a 20 m high rock

* Correspondence: dcdgx07@chd.edu.cn
Department of Geological Engineering, Chang'an University, Xi'an, Shaan'xi, China

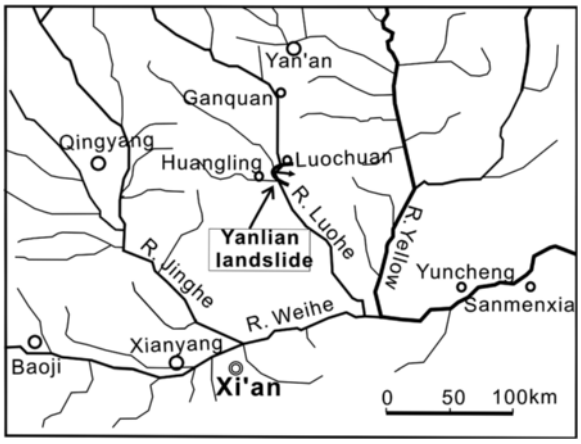

Fig. 1 Location of the Yanlian landslide

Fig. 3 The spring at the toe of the slope

cliff composed of hard horizontal sandstone of the upper Triassic formation. The rock cliff is the base of the third terrace which is overlain by about 2 m thick alluvial pebble and nearly 50 m thick Quaternary loess successively. The pebble is filled with silt-sand and cemented by leached carbonate calcium, so it has a very low permeability. A spring flows out from the top of the pebble with an average flow quantity of about 0.5 L/s (Fig. 3). The sliding mass, shearing out on the pebble bed, is totally loess. Around the failed slope, there are 34 large oil tanks lying on the top and 24 oil pipelines on the toe. A road wanders on the slope from the toe to the top. A boiler house and a coal storehouse stand on the first terrace against the cliff (Fig. 2).

Several days before October 21, 2010, a small part of loess at the toe of slope started to collapse from where a spring flowed out and buried part of the coal storage house. When the workers were trying to clear the collapsed material, the whole slope moved downwards for two days.

The landslide buried part of the coal storehouse (Fig. 2) and cut off all the 24 oil pipelines (Fig. 4) and the road. The oil tanks were only 5 m away from the head scarp (Fig. 5). The refinery had to stop working until 7 days later when the facilities were recovered. There were no fatalities but it caused 700 million RMB losses.

The surface gradient of the slope before failure is about 30° and the vertical height is 47 m. The failure mass has a width of 240 m, a length of 150 m, a thickness of 13.8 m and a total volume of 400,000 m^3. The slope is composed of the unsaturated loess of Late (Q_3 loess), Medium (Q_2 loess) and Early (Q_1 loess) Pleistocene formations as shown in Fig. 6. The groundwater level is only 7 m deep at the center of the landslide, but no groundwater is found in the surrounding slopes. The region is generally shortage of groundwater because of the small precipitation (annually 596 mm/a) and the deep cut landform. The rainfall during the rainy season may quickly run off on the surface. Investigation on the top platform where oil tanks stand finds that there is lots of water vapor released from the pressure adjusters on the heating pipes which are used to keep the oil in the transfer pipes from frozen in winter (Fig. 7). The hot vapor condenses in winter and partly penetrates into the ground. The condensed water of the vapor is possibly the water source in the landslide

Fig. 2 The Yanlian landslide

Fig. 4 The oil transfer pipes cut off by the landslide

Fig. 5 The oil tanks hanging over the top of the head scarp

Fig. 7 The release water vapor from the pressure adjust valves on the heating pipes

which has been ignored at the beginning. Therefore it is assumed that the groundwater in the landslide was generated by unsaturated infiltration of the condensed water drops and the landslide was trigged by the rising of the groundwater level.

Determination of the loess physical properties

The sliding mass and surface are composed of loess. Basic physical properties of loess include permeability, water content, density, plasticity, grain components. The coefficient of saturated permeability was measured through the falling head method. The water content and density were measured by oven drying and metal ring respectively. The plastic limit and liquid limit were measured by hand rolling and Cassgrande apparatus respectively. The results are shown in Table 1. Laser Particle Analysis were utilized to measure the grain size distributions of Q_1, Q_2, Q_3 loess as shown in Fig. 8. It is shown that major component is silt (0.005–0.05 mm) taking up 60 %. The second is clay (<0.005 mm) taking up 20–40 %, and the minor component is fine sand (>0.05 mm) less than 10 %. From Q_3 to Q_2 and Q_1 loess, the mean particle size and the void ratio decrease as well as dry density increases. It demonstrates that the lower the loess layer lies, the longer the time of pedogenesis is and the heavier the load of consolidation experiences, the more compacted the loess is.

Determination of SWCC and HCF

Soil-water characteristic curves (SWCC) were measured in laboratory with undisturbed block specimens of 300 mm × 300 mm × 300 mm in dimensions. The specimens were collected from Q_1, Q_2 and Q_3 loess respectively. The matric suctions were measured in wetting processby the TEN–15 tensiometer and the corresponding moisture contents by the oven-drying method. It was accomplished through the following steps: First, a block of specimen was air dried and a hole of 80 mm in depth and 300 mm in diameter was punched in the center of one face of the specimen. Second, insert a tensiometer into the hole with

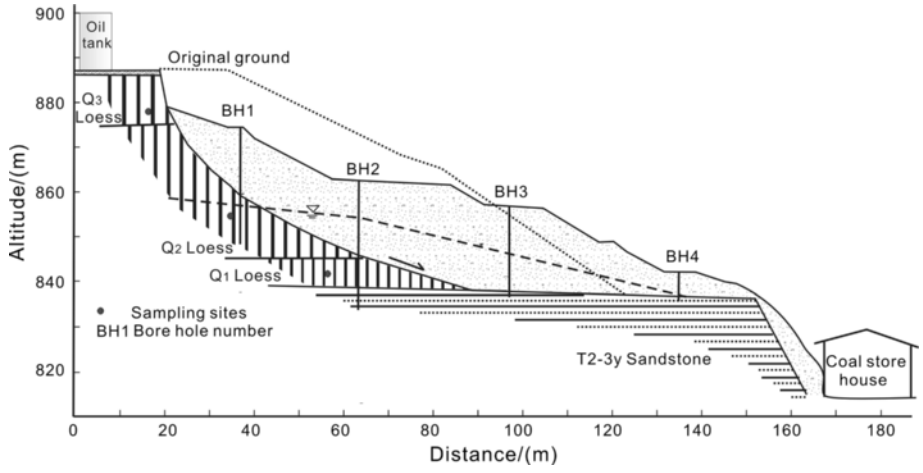

Fig. 6 The main longitude section of the Yanlian landslide

Table 1 The basic physical properties of the loess samples

Loess	Density	Moisture content	Specific gravity	Dry density	Void ratio	Volumetric moisture content	Liquid limit	Plastic limit	Plastic index	Coefficient of permeability
	ρ/(g/cm^3)	w/(%)	Gs	ρ_d/(g/cm^3)	e_0	θ/(%)	w_L/(%)	w_P/(%)	I_P/(%)	k/(m/day)
Q_3	1.67	16.8	2.71	1.43	0.895	24.0	30.9	18.9	12.0	0.110
Q_2	1.86	20.5	2.71	1.54	0.760	31.6	37.0	22.8	14.2	0.044
Q_1	1.89	19.9	2.71	1.58	0.715	31.4	33.7	20.8	12.9	0.027

the ceramic head saturated in advance and fill the gap with the same soil powder. Third, the specimen was enclosed with melted wax to make the moister distribution uniform. Some time later, read the data when the matric suction recorded by the gauge is stable. Then remove part of the enclosed wax and collect a bit of soil to measure the water content. So a set of data was obtained. In the next cycle, dropped some water in the specimen and enclosed it again. Repeat the above process to get a new set of data till the suction is 0.

Because the range of tensiometer is less than 100 kPa, the measured data is applied to regress with the Fredlund & Xing's (1994) eq. (1) to extend the curves to a higher suction range:

$$\theta_w = C(\psi)\frac{\theta_s}{\{\ln[e+(\psi/a)^n]\}^m} \quad (1)$$

Where θ_w is the volumetric moisture content; θ_s is the saturated volumetric moisture content; ψ is the matric suction; a is the approximate air-entry value of the soil; n is a parameter that controls the slope at the inflection point in the SWCC; m is a parameter related to the residual moisture content; e is the natural number, 2.71828; and $C(\psi)$ is the correcting function defined by eq. (2).

$$C(\psi) = 1 - \frac{\ln\left(1+\frac{\psi}{C_r}\right)}{\ln\left(1+10^6/C_r\right)} \quad (2)$$

Where C_r is a constant related to the matric suction corresponding to the residual volumetric moisture content, a typical value for it is 1500 kPa.

The best fitting values of the parameters a, m, n and the regressed SWCC are shown in Fig. 9, in which the dots are the measured values with tensiometer.

The hydraulic conductivity functions (HCF) is estimated empirically by the model proposed by Childs and Collis-Gorge (1950) and improved by Marshall (1958) and Kunze et al. (1968). The procedure is performed by dividing SWCC into n equal moisture content increments. The relationship between the HCF and the matric suctions is calculated by the model. With the measured saturated coefficients of permeability in Table 1 and the SWCC curves in Fig. 9, the HCF are predicted and shown in Fig. 10.

Measurement of the unsaturated strength parameters c_0', φ' and φ^b

Fredlund et al. (1978) unsaturated shearing strength is expressed as eq. (3).

$$\tau_f = c_0^{'} + (\sigma - u_a)\tan\phi^{'} + (u_a - u_w)\tan\phi^b \quad (3)$$

Where τ_f is the unsaturated shearing strength; c'_0 is the effective cohesion; ϕ' is the effective friction angle; σ-u_a is the pure normal strength; u_a-u_w is the matric suction and ϕ^b is the friction angle related to matric suction.

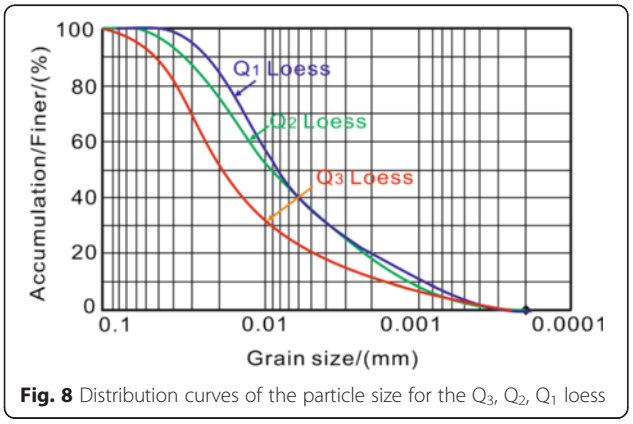

Fig. 8 Distribution curves of the particle size for the Q_3, Q_2, Q_1 loess

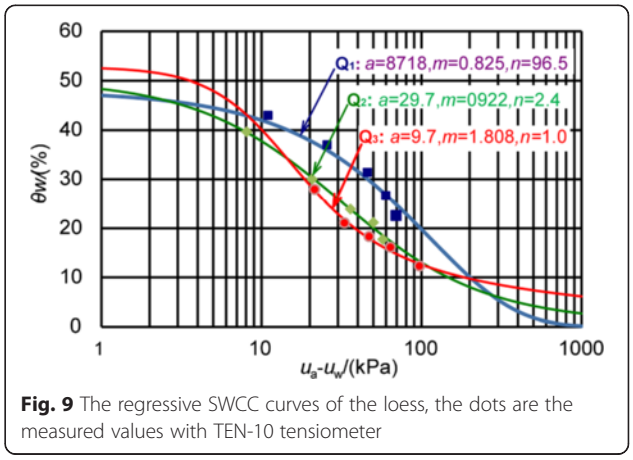

Fig. 9 The regressive SWCC curves of the loess, the dots are the measured values with TEN-10 tensiometer

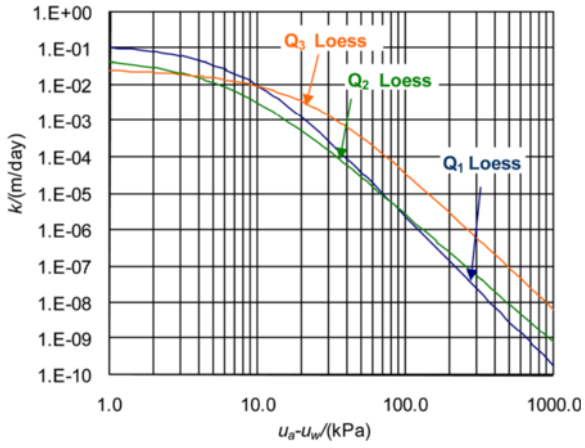

Fig. 10 The HCF curves of the Q_3, Q_2, Q_1 loess

In which, c'_0 and ϕ' can be measured by conventional direct shear test or triaxial test with saturated specimens. ϕ^b can be measured by suction-controlled direct shear test or triaxial test.

Let

$$c' = c'_0 + (u_a - u_w)\tan\phi^b$$

Where, c' can be considered as the total cohesion which includes the friction produced by matric suction. So, there is

$$\tan\phi^b = \frac{c' - c'_0}{u_a - u_w} \tag{4}$$

Here the total cohesion c' can be determined against u_a-u_w by the conventional direct shear test or triaxial test.

For the three layers of Q_3, Q_2 and Q_1 loess as shown in Fig. 6, Q_3 lies on the top of the slope and fails due to the tension cracks, so Q_3 loess should have lost its strength before the slope failure. Q_2 loess fails at a shear zone in the middle of the slope, so consolidated-undrained triaxial tests for Q_2 loess were conducted to simulate the stress state. Q_1 loess shears outward on the top of the pebble bed horizontally which has a fixed shear direction, so consolidated quick direct tests were conducted on Q_1 loess to simulate the confined shear plane.

The moisture content of the loess underground is generally above 5 % while the saturated moisture content is about 30 %. Specimens with initial moisture contents of 5, 10, 15, 20, 25 and 30 % were prepared for Q_2 loess and Q_1 loess repectively to do the laboratory tests. To make the specimen with intended moisture content, shape and dry each specimen first, then put it on a balance and drop water around it till the total weight is equivalent to the moisture content. After that, the specimens are enclosed in a rubber membrance for a week at least to make the moisture distribution uniform.

Triaxial tests for Q_2 loess were performed on the specimens of 80 mm in height and 39 mm in diameter. The confining pressures were set at 100 kPa, 200 kPa, 300 kPa, 400 kPa and 500 kPa rspectively. The rate of axial displacement was set at 0.04 mm/min for all the tests. Direct shear tests for Q_1 loess were conducted using the disk specimens of 20 mm in height and 50 mm in diameter. Normal stress was applied with 100 kPa, 200 kPa, 300 kPa, 400 kPa, 500 kPa, 600 kPa and the shear displacement rate was set at 0.02 mm/min.

The triaxial test results are showned in the forms of the maximam shear stress $q = (\sigma_1\text{-}\sigma_2)/2$ against axial strain ε_1 and q against average principle stess $p = (\sigma_1 + \sigma_2)/2$ in Fig. 11. It can be seen that the specimens with moisture contents lower than 10 % have no pore watetr presure produced in the whole shearing process, but those with higer moisture contents produce pore water presure. The higher the moisture content, the higher the pore water presure is. Specimens with 5 % moisture contents have remarkable peak values than that of 10 % moisture contents under low confining pressure of 100 kPa. Meanwhile, most of the other specimens have realistic elasto-plastic and hardening stress–strain forms. Some of the high moisture content specimens have gentle softening stress–strain curves, while the strain soften can be attributed to the increase of pore water pressure. It manifests that the loess could maintain the stuctural strength in the condition of low moisture content and low confning pressure. For high moisture content and high confining pressure, the stucture would be broken during consolidation prior to shearing.

With the stress path q-p curves, the effective strength K_f lines can be drawn as the common tangent lines of effective stress paths, and the total effective cohesion c' and friction angle ϕ' can be calculated by intercept b and gradient angles α of K_f lines with eq. (5). The obtained unsaturated strength parameters, the moisture contents, the calculated volumetric moisture contents and the matric suction obtained from the SWCC curves are listed in Table 2.

$$\begin{aligned} c' &= b\cos^{-1}\phi' \\ \phi' &= \sin^{-1}(\tan\alpha) \end{aligned} \tag{5}$$

Where b is the intercept and α is the gradient of K_f line respectively.

The data in Table 2 shows that the effective friction angle ϕ' is independent of the moisture content. The range of the angles is between 24.5° and 25.5°. The mean

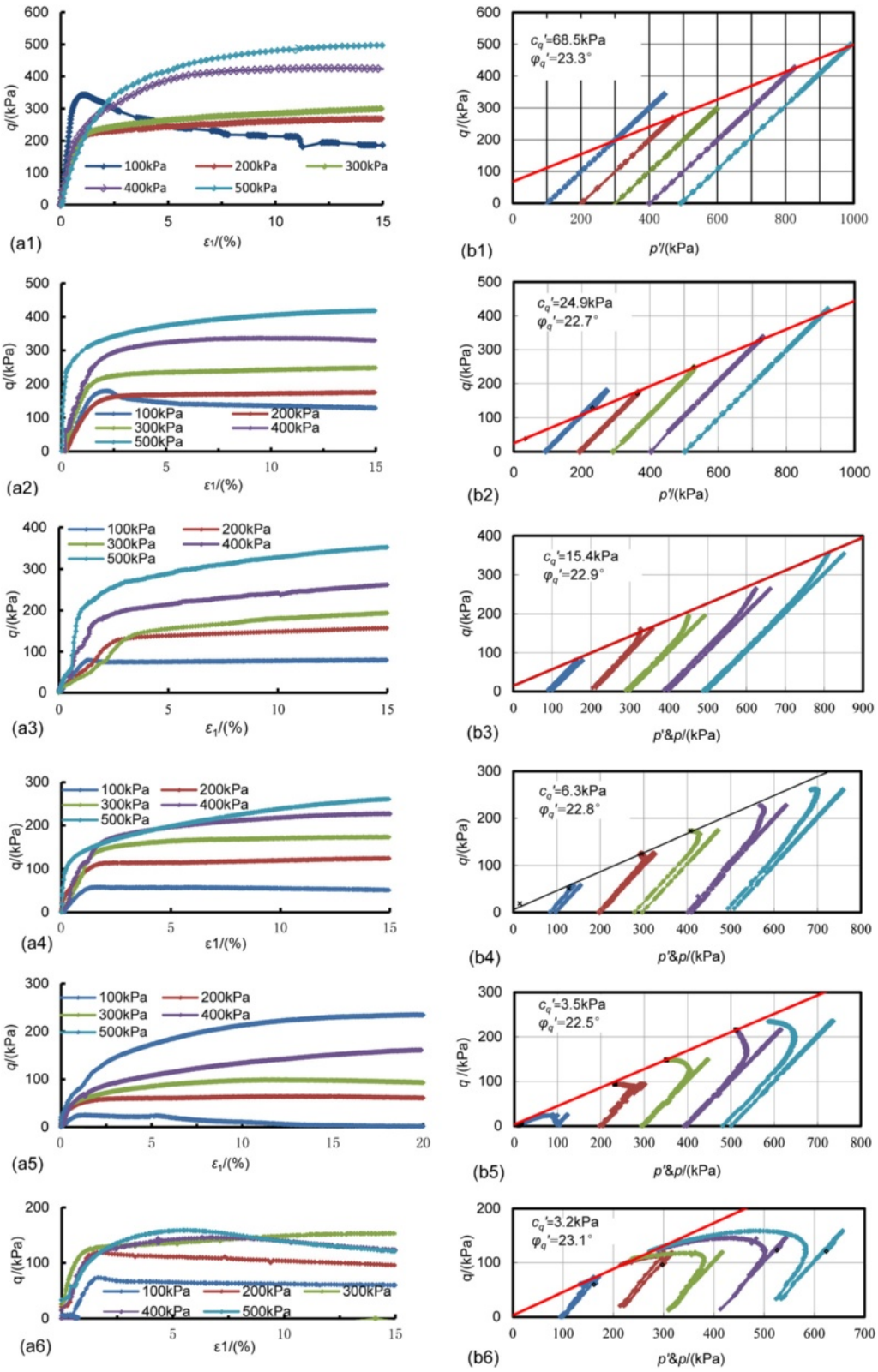

Fig. 11 Stress–strain curves and stress paths for the specimens of definite moisture contents (a1)-(a6) are the q-ε_1 curvesand (b1)-(b6) are the stress path q-p curves for the specimens with $w = 5$, 10, 15, 20, 25, 30 % respectively, wherein $q = (\sigma_1\text{-}\sigma_2)/2$, $p = (\sigma_1 + \sigma_2)/2$

Table 2 The measured effective strength parameters and the relevant indexes for Q_2 loess

Specimen no.	Moisture content	Volumetric moisture content	Matric suction	Total effective cohesion	Effective friction angle
	w/(%)	θ_w/(%)	U_a-u_w/(kPa)	c'/(kPa)	φ'/(°)
T_1	5	7.7	200.5	74.6	25.5
T_2	10	15.4	67.0	27.0	24.8
T_3	15	23.1	28.7	16.7	25.0
T_4	20	30.8	10.6	6.8	24.9
T_5	25	38.5	0.2	3.8	24.5
T_6	30	46.2	0.0	3.5	25.2
Strength parameters			$\varphi^b = 19.5°$	$c'_0 = 3.50$ kPa	$\varphi' = 25.0°$

value is $\phi' = 25.0°$. The total effective cohesion c' has a reverse relation with the moisture content. It decreases prominently in the low moisture content range. As the moisture content exceeds the plastic limit (PL = 22.8 %), it reaches to its minimum value 3.50 kPa or so and keeps constant. So c'_0 is accepted as 3.50 kPa.

The curve of c'-c'_0 verse u_a-u_w, shown in Fig. 12, expresses that the relationship of c'-c'_0 and u_a-u_w is linear and the gradient angle of the linear curve is 19.5°.

The stress–strain curves of the direct shear for Q_1 loess are shown in Fig. 13. It can be seen that the marked peak values appear in the cases of low normal stresses and low moisture contents, such as in the moisture contents of 5 % and 10 % under normal stress from 100 kPa to 400 kPa. For the remaining specimens, the stress-strains show realistic elasto-plastic behavior or hardening, similar to the triaxial results of Q_2 loess. Assuming 6 mm shear displacement as the failure point, the shear strength against mormal stress for each moisture content are ploted in Fig. 14, from which the total effective cohesions c' and effective friction angles ϕ'can be calculated by eq. (5) and are listed in Table 3. The moisture contents, the calculated volumetric moisture contents and the matric suction determined by SWCC curves are also listed in Table 3.

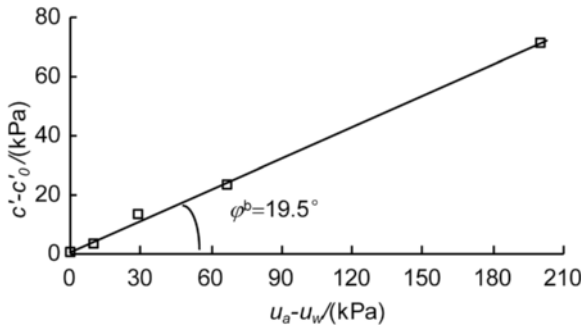

Fig. 12 The relation between c'-c'_0 against u_a-u_w of the Q_2 loess

Similar to the triaxial results for Q_2 loess, the effective friction angle is independent of the moisture content. The range of the angles is between 29.4° and 30.5°. The mean value is $\phi' = 30.0°$. The total effective cohesion decreases with the increase of the moisture content and changes prominently in the low range. It reaches to the minimum value of 5.0 kPa or so as the moisture content decreases to plastic limit (PL = 20.8 %). So $c'_0 = 5.0$ kPa. Through the curve of c'-c'_0 verse u_a-u_w as shown in Fig. 15, ϕ^b can be determined to be 25.3°.

Analysis for the landslide initiation mechanism

To analyze the initiation mechanism of the landslide, a 2D FEM model of the slope before failure is built up to simulate the water seepage processes and to monitor the moisture field. The stress field and the strength variation with the moisture change are also analyzed. Fig. 16 shows the FEM model. Geo-studio SEEP and SIGMA software are utilized to simulate the seepage process and the stress fields, respectively.

The HCF of Q_1, Q_2, Q_3 loess, the SWCC and the related strength parameters of Q_1, Q_2 loess have been fully documented above. The strength of Q_3 loess can be neglected, so a low cohesion is assigned to it empirically and the friction angle is taken as zero. The deformation parameters of elastic module and Poisson's ratio have minor effect on the stress field, so values of these parameters for all the strata are assigned empirically. The strength of the bedrock is much higher than the loess strata, so a high cohesion and friction angle are assigned. The values for all the parameters needed in the simulation are summarized in Table 4.

The initial condition starts as water begins to drop in the zone of the oil tanks standing on top of the slope. By estimating the voulme of the dropping water into the ground in winter, a 20 mm high and 5 m wide water column is supposed to seep into the ground perday and continue for 100 days (winter days) a year. The rainfall is negleted. In addition, the initial moisture contents of the loess layers are defined by the moister content logging in the borehole in the nearby slope.

Geo-studio SEEP is used to simulate the seepage processes. The moisture field (expressed as pore water pressure field) is added into the Geo-studio SIGMA to simulate the stress and the strength variation under water infiltration. The sliding surface is fixed as the real occurred one, and the shear stress as well as shear strength at each point on the sliding surface can be figured out with the simulated stress states. The factor of safety Fs is defined by eq. (6) based on limit equilibrium theory.

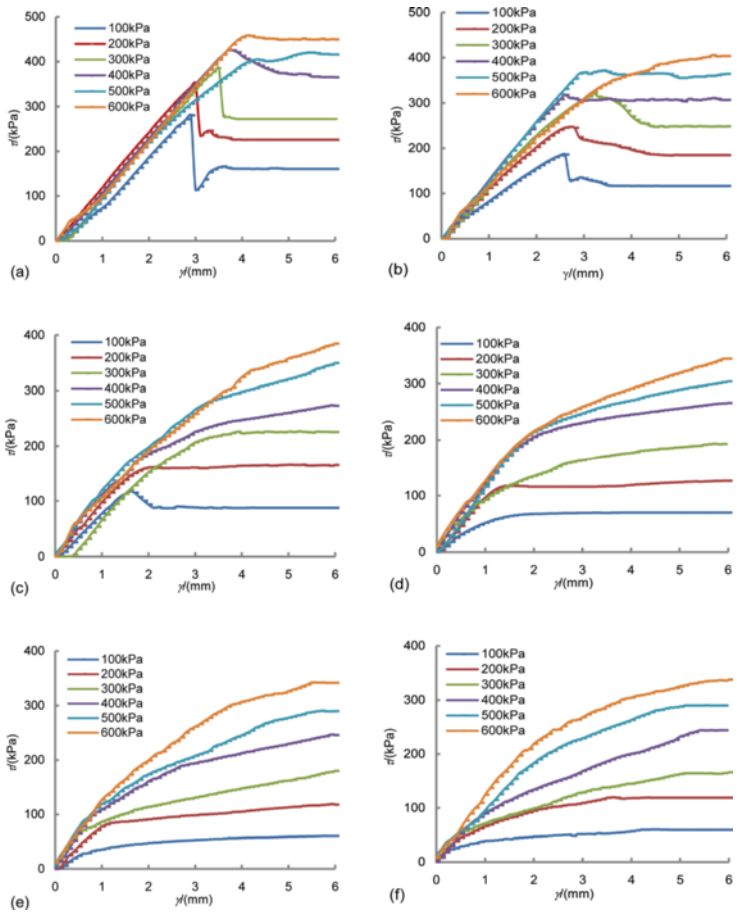

Fig. 13 The shear stress–strain curves of the test results for different moisture contents (**a**)$w = 5$ %; (**b**)$w = 10$ %; (**c**)$w = 15$ %; (**d**)$w = 20$ %; (**e**)$w = 25$ %; (**f**)$w = 30$ %

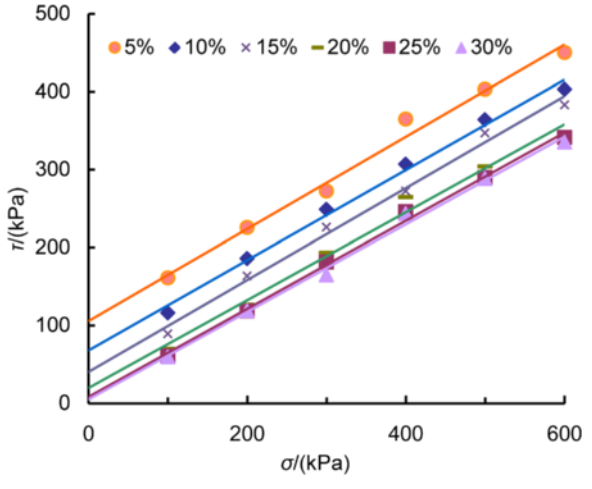

Fig. 14 The shear strength vs normal stress for different moisture contents

Table 3 The measured effective strength parameters and the relevant indexes for Q_1 loess

Specimen no.	Moisture content	Volumetric moisture content	Matric suction	Total effective cohesion	Effective friction angle
	w/(%)	θ_w/(%)	u_a-u_w/(kPa)	c'/(kPa)	φ'/(°)
D_1	5	7.9	225.2	105.7	30.0
D_2	10	15.8	116.9	67.9	30.1
D_3	15	23.7	60.3	42.0	30.5
D_4	20	31.6	24.3	19.4	29.4
D_5	25	39.5	0.0	7.9	29.6
D_6	30	47.4	0.0	5.0	29.5
Strength parameters			$\varphi^b = 25.3°$	$c'_0 = 5.0$ kPa	$\varphi' = 30.0°$

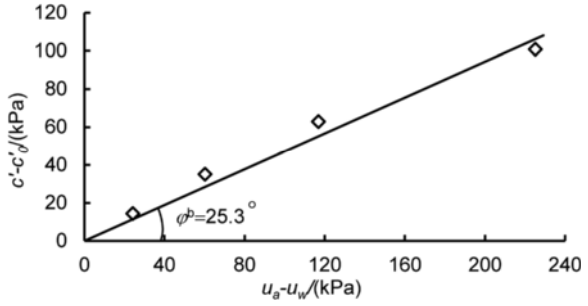

Fig. 15 Relation between c'-c'_0 and u_a-u_w of the Q_1 loess

$$Fs = \frac{\int_{x_A}^{x_B} \tau_f dx}{\int_{x_A}^{x_B} \tau dx} \quad (6)$$

Where τ_f is the shear strength of the sliding surface as defined by eq. (3); τ is the shear stress on the sliding surface; x_A and x_B are the horizontal coordinate of the end points of the sliding surface.

The simulations are conducted from the beginning of water dropping and the factor of safety is calculated as well till it fails. At last, it keeps stable for 15 years before failure. The period is agreement with the age of the oil tanks.

Figure 17 shows the simulated pore water pressure fields at specified time. For each year, the results at the ends of 100 days water dropping and after 265 days break are provided. It shows that in the first year, the moisture perches at the upper layer of the slope. And when stopping infiltrating, the moisture scatters and negative pore pressure decreases. In the 4th year, moisture moves down to the impermeable rock bed and migrates along the boundary of Q_3 and Q_2 loess as well as the bedrock. When the infiltration stops, the wetting front moves laterally and the groundwater level decreases with the water extends outwards. However, at this time, just a little moisture invades the sliding surface, so the slope stability has no significant change. In the 9th year, the groundwater rises up to submerge the lower portion of the sliding surface and the slope stability starts to decrease. During the drop break, the groundwater continues flowing from the inner to the slope toe. As a result the groundwater level beneath the slope toe continues rising. So in all the yearly periods, the slope stability becomes worse even after the water stops infiltrating.

Figure 18 shows the evolution of the factor of safety during water infiltration. During the first eight years, the factor of safety has no prominent decreasing and begins to lower in the 9th-10th years. The time coincides with the period that the groundwater level begins to touch the potential sliding surface and rises continuously. In addition, the moisture content of the slope above the groundwater level also increases which reduces the strength of the loess. All of these factors lead to the slope failure.

Table 4 The values of the parameters for the slope simulation

Strata	Q_3 loess	Q_2 loess	Q_1 loess	Sandstone
Elastic module E/(kPa)	10^2	10^3	10^3	10^5
Poisson's ratio v	0.35	0.35	0.33	0.20
Effective friction angle φ'/(°)	0.0	25.0	30.0	45.0
Friction angle related to suction φ^b/(°)	0.0	195.	25.3	-
Saturated effective cohesion c'_0/(kPa)	3.0	3.5	5.0	1000
Density γ/(g/cm^3)	1.65	1.86	1.89	2.45
Saturated permeability K/(m/d)	0.110	0.044	0.027	-
Initial moisture content w_0/(%)	16.8	20.5	19.9	-
Initial volumetric moisture content θ_0/(%)	24.0	31.6	31.4	-
Initial matric suction (u_a-u_w\)$_0$/(kPa)	18.3	9.2	25.1	-

Conclusions

Loess is a typical unsaturated soil which is sensitive to moisture. In this paper, investigation demonstrates that

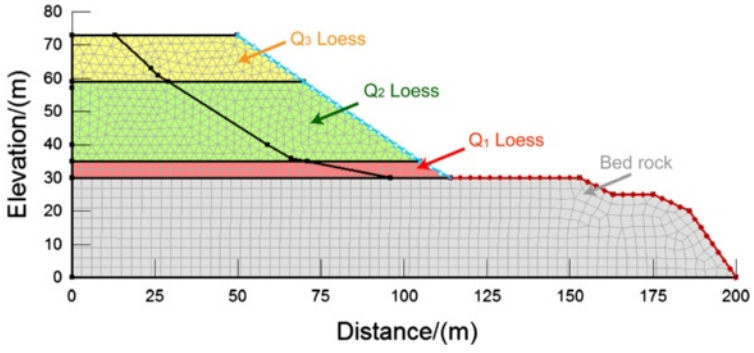

Fig. 16 FEM meshes of the slope model before failure ($Fs = 1.44$)

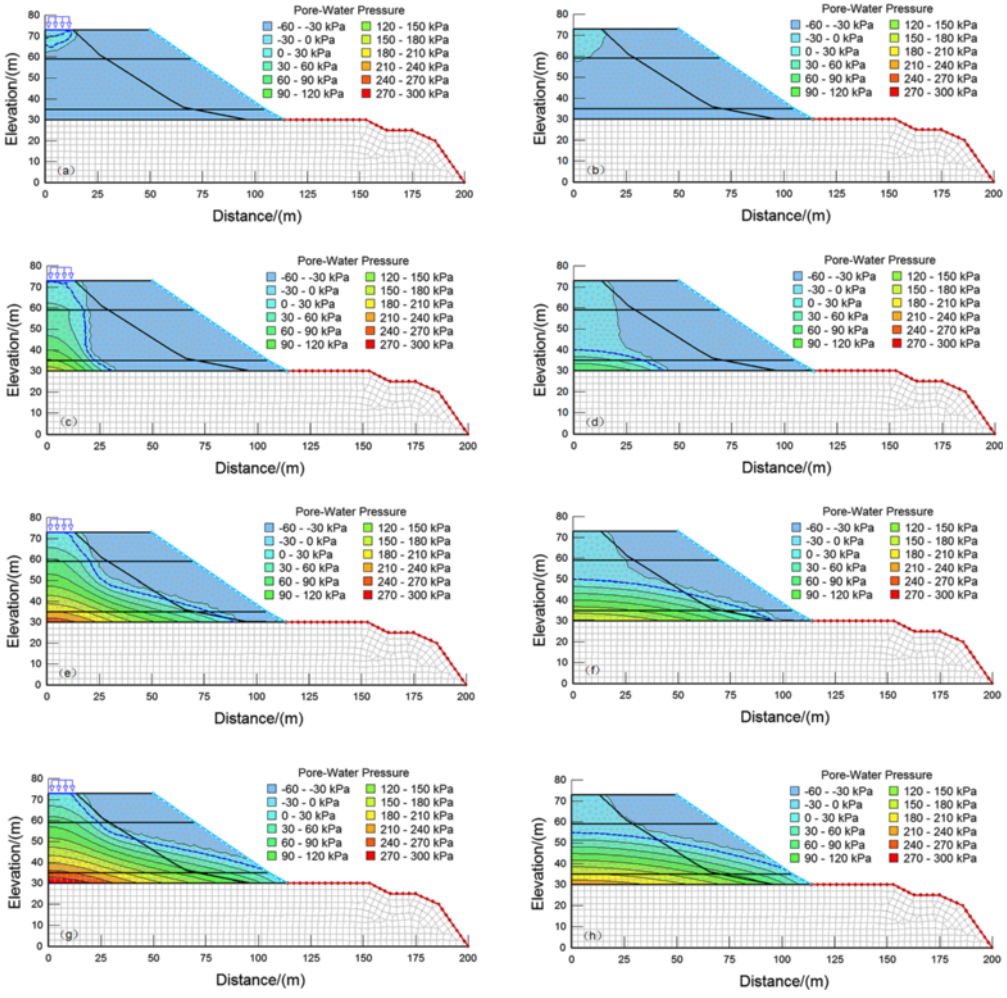

Fig. 17 The simulated results of the pore water pressure in the slope at different times (**a**) At the end of 100 days, *Fs* = 1.43; (**b**) At the end of the first year, *Fs* = 1.43; (**c**) At the end of the 4th year and 100 days, *Fs* = 1.44; (**d**) At the end of the 5th year, *Fs* = 1.43; (**e**) At the end of the 9th year and 100 days, *Fs* = 1.36; (**f**) At the end of the 9th year, *Fs* = 1.29; (**g**) At the end of the 14th year and 100 days, *Fs* = 1.03; (**h**) At the end of the 14th year, *Fs* = 1.01

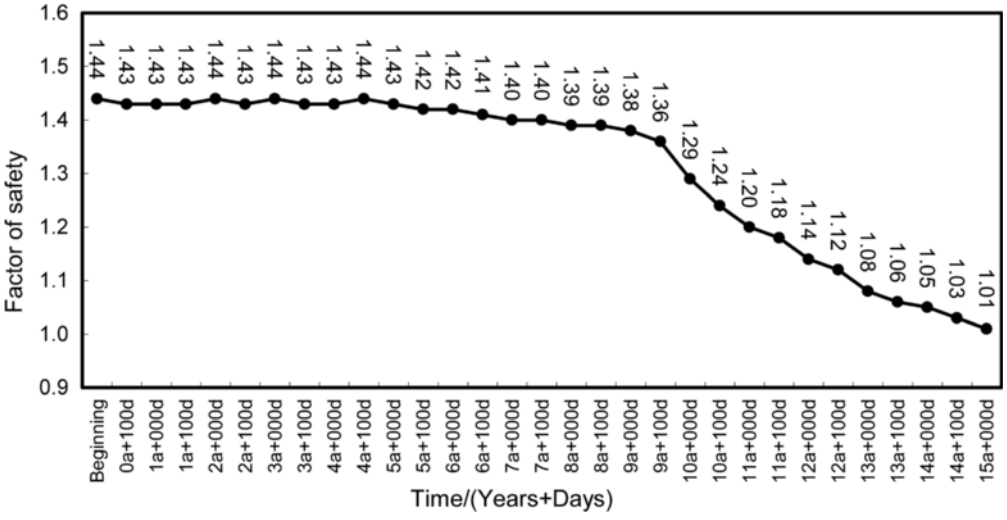

Fig. 18 The factor of safety varied with time

long term condensed water vapor released from the pressure adjusters on the heating pipes which are used to keep the oil in the transfer pipes from frozen in winter is the triggering factor of the Yanlian landslide. Laboratory tests including conventional triaxial tests, consolidation quick shear tests and SWCC measurement are performed to estimate the unsaturated strength parameters and water conductivity.

The safety of factor can be figured out based on the moisture field and the stress field simulated by the FEM model with the parameters. The result shows that a little water infiltration has minor effects on slope stability for some time. As a result it is easy to be ignored. However, when the period of water infiltration is long enough to raise the groundwater level, it will have detrimental influence on the stability and the slope will fail at last. The analysis above illustrates that any minor water produced by engineering or other activities may have harmful effect on slope stability for a long period of action. Therefore it is essential to take account of this kind of water and adopt measures to curb the surface water infiltration and to drain the groundwater.

Competing interests
The authors declare that they have no competing interests.

Authors' contributions
All authors participated the field investigations. HS & XZ conducted sampling and all the laboratory tests. XZ conducted graphing and analysis for the test results. HS conducted the numerical simulations. PL drafted the manuscript. All authors read and approved the final manuscript.

Acknowledgements
This research was funded by one of National Basic Research Program of China (2014CB744701) and National Natural Science Foundation of China (Program no. 41372329). The authors wish to acknowledge Dr. Austin ChukwuelokaOkeke, Department of Geoscience, Shimane University, for reading the manuscript and revising the English language. Our thanks also give to Dr. Xianli Xing, Department of Geological Engineering, Chang'an University, for her valuable guidance of the laboratory tests.

Received: 7 October 2014 Accepted: 27 April 2015
Published online: 17 September 2015

References

Bai MZ, Du YQ, Kuang X (2012) Warning Method and System in Risk Management for Loess Engineering Slopes. J Perform Constr Facil 26(2):190–196
Chillds EC, Collis-Geoge GN (1950) The permeability of porous materials. Proc R Soc London, Ser A 201:392–405
Dai FC, Lee CF (2001) Frequency-volume relation and prediction of rainfall-induced landslides. Eng Geol 59(3/4):253–266
Fredlund DG, Morgenstern NR, Widger RA (1978) The shear strength of unsaturated soils. Can Geotech J 15:313–321
Fredlund DG, Xing A (1994) Equations for the soil-water characteristic curve. Can Geotech J 31(3):521–532
Kunze RJ, Uehara G, Graham K (1968) Factors important in the calculation of hydraulic conductivity. Soil Sci Soc Am Proc 32:760–765
Lei XY (1994) The hazards of loess landslides in the southern tableland of Jingyang County, Shaanxi and their relationship with the channel water into fields (In Chinese). J Eng Geol 3(1):56–64
Li P, Zhang B, Li TL (2012) Study on Regionalization for Characteristic and Destruction Rule of Slope in Loess Plateau (In Chinese). J Earth Sci Environ 34(3):89–98
Li TL, Wang P, Xi Y (2013). Mechanisms for initiation and motion of Chinese loess landslides, Ed. by FawuWang, Masakatsu Miyajima, Tonglu Li,Wei Shan, Teuku Faisal Fathani, Progress of Geo-Disaster Mitigation Technology in Asia, Springer, Verlag Berlin Heidelberg:105-122.
Liao HJ, Su LJ, Li ZD, Pan YB, Fukuoka H (2008) Testing study on the strength and deformation characteristics of soil in loess landslides. Ed. by Chen Zuyu, Zhang Jianmin, Li Zhongkui, Wu Faquan, Ho Ken, Landslides and Engineered Slopes (from the Past to the Future), CRC Press, Leiden, The Netherlands, Vol 1:443-447.
Marshall TJ (1958) A relation between permeability and size distribution of pores. J Soil Sci 9:1–8
Tu XB, Kwong AKL, Dai FC, Tham LG, Min H (2009) Field monitoring of rainfall infiltration in a loess slope and analysis of failure mechanism of rainfall-induced landslides. J Eng Geol 105(1):134–150
Zhang JQ, Peng JB (2014) A coupled slope cutting—a prolonged rainfall-induced loess landslide: a 17 October 2011 case study. Bull Eng Geol Environ 73(4):997–1011